

Article

Magnesium Alloy Scrap Vacuum Gasification—Directional Condensation to Purify Magnesium

Rui Li ^{1,2,3}, Lipeng Wang ^{1,2}, Bin Yang ^{1,2,3,4}, Baoqiang Xu ^{1,2,3}, Dong Liang ^{1,4}, Fei Wang ^{1,2,3,4} and Yang Tian ^{1,2,3,4,*}

- ¹ Key Laboratory for Nonferrous Vacuum Metallurgy of Yunnan Province, Kunming University of Science and Technology, Kunming 650093, China
- ² National Engineering Research Center of Vacuum Metallurgy, Kunming University of Science and Technology, Kunming 650093, China
- ³ Engineering Research Center of Aluminium Industry of Yunnan Province, Kunming University of Science and Technology, Kunming 650093, China
- ⁴ Faculty of Metallurgical and Energy Engineering, Kunming University of Science and Technology, Kunming 650093, China
- * Correspondence: emontian@hotmail.com; Tel.: +86-138-8880-5314

Abstract: Magnesium alloys, known as a “21st-century green engineering material”, are widely used in many fields, including during the production and consumption of magnesium alloys die-casting products such as AZ91D, AM50, and AM60B. In addition, a large amount of waste is generated, which not only pollutes the environment but also wastes secondary resources. Hereby, we reported the vacuum gasification—directional condensation method, calculated the vapor pressure separation coefficient parameters, and drew the gas-liquid phase equilibrium diagram depending on the distillation temperature, condensation temperature, and system pressure for the magnesium volatilization process. The results showed that under the following conditions (distillation temperature: 1073 K, system pressure: 100 Pa, condensation temperature: 873 K, and condensation duration: 30 min), the magnesium volatilization yield could approach 93.76%, and the purity of magnesium could reach 99.98%. This research is a good theoretical and practical basis for the recovery of magnesium alloy waste using the vacuum gasification method.



Citation: Li, R.; Wang, L.; Yang, B.; Xu, B.; Liang, D.; Wang, F.; Tian, Y. Magnesium Alloy Scrap Vacuum Gasification—Directional Condensation to Purify Magnesium. *Metals* **2023**, *13*, 675. <https://doi.org/10.3390/met13040675>

Academic Editor: Fernando Castro

Received: 27 February 2023

Revised: 26 March 2023

Accepted: 28 March 2023

Published: 29 March 2023



Copyright: © 2023 by the authors. Licensee MDPI, Basel, Switzerland. This article is an open access article distributed under the terms and conditions of the Creative Commons Attribution (CC BY) license (<https://creativecommons.org/licenses/by/4.0/>).

Keywords: vacuum gasification; magnesium alloy scrap; purification

1. Introduction

Magnesium and magnesium alloys are known as “21st-century green engineering materials” [1] and “revolutionary medical metal materials” [2]. They have very broad application prospects in the fields of transportation, aerospace, electronics industry, battery and biomedical (new medical metal materials and implantation device research) [3–9], etc. Against a backdrop of carbon peak and neutrality targets background, magnesium alloy becomes an important material for automotive lightweight manufacturing, which has important strategic significance in promoting sustainable development [10]. However, a large amount of waste is generated during the production and consumption of magnesium alloys. Magnesium alloy products only account for 30–40% of the input materials, and the remaining 60–70% become wastes in different forms [11]. The scrap usually contains a large number of oxides, Zn, Al, Fe, Cu, Ni, Si, and other impurity elements, which significantly reduce the corrosion resistance and promote magnesium alloy mechanical properties. If wastes are directly discarded, they not only pollute the environment but also waste valuable metal resources. The energy required to recycle Mg alloy scrap is only about 5% of that required to produce the same amount of primary material (3 kW-h/Kg-Mg) [12], and recovery capacity can reach 100%. Therefore, effectively recycling scrap magnesium alloy can not only notably reduce the cost of magnesium alloy die casting but also can greatly extend the life cycle of magnesium alloy, which is of great practical significance

for the realization of resource recycling and the development of a resource-saving and environment-friendly society.

At present, the main methods of magnesium alloy purification are the melt refining method [13], zone melting method [14], vacuum method [15], etc. Roberto Lucci [16] used a secondary melt refining method to recover AZ91D chips. This method added a refining flux while passed argon gas at the same time, the iron and manganese content was reduced by two refining steps, and the recovery rate reached 90%. However, this method relies mostly on chloride, and corrosive gases such as Cl_2 and HCl which will be released in refining, it not only corrodes the production equipment but also pollutes the environment [17]. At the same time, the addition of solvents leads to the production of new inclusions and reduces the physical properties of magnesium alloys. U. Rambabu [18] reduced the impurities such as Fe, Cu, and Zn from 0.00090% to 0.00004% by regional melting in gallium and purified gallium from 99.99% to 99.99995%. However, the regional melting method is more effective in metal purification, it needs to be repeated several times, and magnesium is volatile and easily oxidized, so it is difficult to product purity magnesium by regional melting.

As an emerging metallurgical technology, the vacuum method has the advantages of simple resource equipment, short process flow, strong controllability, high purity of recovered products, and environmental friendly, which is widely used to prepare high-purity metals, including some rare metals [19–22], among them, the vacuum method can change the magnesium phase and condensation product morphology by controlling the vapor pressure. It is divided into the vacuum gasification and distillation methods [23]. The main distinction is that the phase transition process is different, in which vacuum gasification is a process of direct transformation from solid to gas at high vacuum and low temperature, while vacuum distillation is the process of changing from solid to liquid to gas at low vacuum and high temperature. Li [24] used 4N magnesium as the raw material and controlled the condensation temperatures of 450 °C, 650 °C and 700 °C in the upper, middle, and lower sections of the distillation tower, respectively, and a small amount of 5N high-purity magnesium was obtained at the distillation temperature of 700–750 °C. However, research on raw magnesium alloy waste is rarely reported, and magnesium and zinc are difficult to effectively separate, which has become a stumbling block for magnesium alloy purification. In this paper, the purification of magnesium alloy scrap was carried out by the vacuum gasification method, as shown in Figure 1. The waste magnesium alloy can be recovered efficiently under a high vacuum. Firstly, the saturated vapor pressure and separation coefficient were calculated in the magnesium alloy scrap, and then the vacuum gasification experiment was carried out to separate the magnesium alloy scrap. This research can lay a theoretical and practical foundation for the vacuum recovery of magnesium alloy waste.

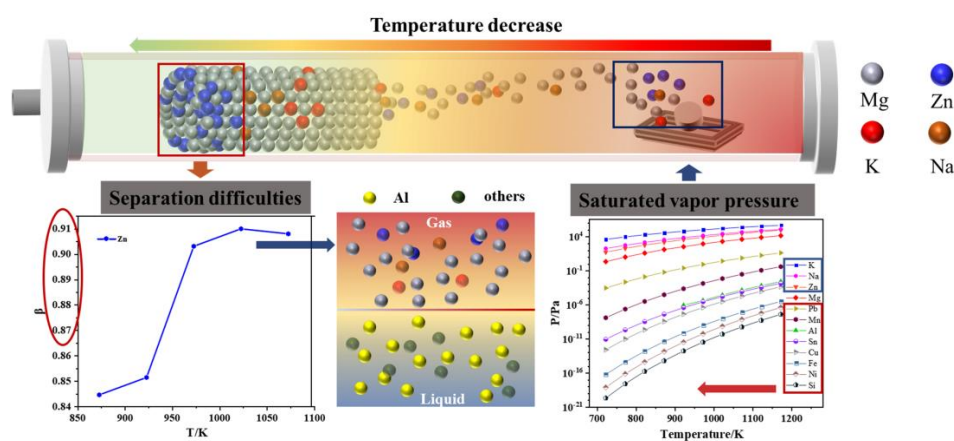


Figure 1. Schematic diagram of the purification of magnesium by vacuum gasification-directed condensation method.

2. Theoretical Analysis

2.1. Saturation Vapor Pressure

Under certain conditions, the solid or liquid state of various substances tends to become gaseous, and the gaseous state also tends to become a solid or liquid state. At a specific temperature and pressure, the gas state of a substance and its solid and liquid states will achieve dynamic balance. This pressure is the saturated vapor pressure at this temperature.

The saturated vapor pressure of a metal represents the volatile properties of the metal at a certain temperature. For the gas-liquid (or gas-solid) phase equilibrium of pure matter, the relationship between pressure and temperature is expressed by Equation (1).

$$\frac{dp}{dT} = \frac{\Delta H_m^*}{T(V_{m,g} - V_{m,l})} \quad (1)$$

In Equation (1), P is the saturated vapor pressure of the liquid metal, Pa; T is the temperature of the liquid metal, K; ΔH_m^* is the latent heat of evaporation of liquid metals, J/mol; $V_{m,g}$ and $V_{m,l}$ are the molar volumes of metals in gaseous and liquid, respectively, m^3/mol .

At low pressure, Metal vapor can be regarded as an ideal gas, $V_{m,l}$ can be ignored. At this time, $pV = nRT$, Equation (1) can be integrated as:

$$\frac{d \ln p}{dT} = \Delta H_m^* / RT^2 \quad (2)$$

Due to the latent heat of liquid evaporation, it is related to temperature, and its relationship can be expressed as $\Delta H_m^* = \Delta H_0 + aT + bT^2 + CT^3 + \dots + \text{constant}$, by integrating Equation (2) and substituting A , B , C , and D for various coefficients, we can attain the relationship between saturated vapor pressure and temperature [25], Equation (3):

$$\lg p^* = A/T + B \lg T + CT + D \quad (3)$$

The saturated vapor pressure of each component in the magnesium alloy can be calculated from Equation (3). As shown in Figure 1, metal saturation vapor pressure increased with the rise of temperature, and K, Na, and Zn are higher than the pressure of Mg. Other impurities are lower than the pressure of Mg, which indicates that Mg enters the gas phase, and other impurities enter the liquid phase, and it can be separated from most of the impurities in magnesium scrap. At the same time, Zn and Mg saturated vapor pressure differences are smaller, which tend to parallel, and it shows that their separation is not easy. Thus, the order of volatile elements is $K > Na > Zn > Mg > Pb > Mn > Al > Sn > Cu > Fe > Ni > Si$, which is also the order in that impurities are removed under vacuum conditions.

2.2. Separation Coefficients

The difference between the vapor pressure of the alloy with pure metal vapor pressure is the separation coefficient. Each component in the alloy volatilizes to different degrees. Each of the gases has a certain proportion, which is related to the purity of the main metal during metal purification. In order to study the separation process of the alloy degree, the separation coefficient is introduced. The separation coefficient of A-B binary alloy (β_A) can be expressed by Equation (4),

$$\beta_A = \frac{P_A^* \times \gamma_A}{P_B^* \times \gamma_B} \quad (4)$$

where P_A^* and P_B^* are the saturated vapor pressures of components A and B; γ_A and γ_B are the activity coefficients of components A and B, respectively.

The separation coefficients of impurities at different temperatures are shown in Table 1. It can be seen that β_{Zn} tends to be 1 at the four temperatures, which indicates that the separation of Mg and Zn is difficult. However, the separation coefficient β_i of the remaining impurities is much less than 1, and it shows that the remaining impurities and Mg are easy

to separate. Figure 2 shows the gas-liquid equilibrium diagram of the Mg-i binary system. It can be seen from Figure 2b that the magnitude difference between the liquid and gas phase contents of Zn is very small, and the gas-liquid equilibrium lines almost overlap at the four temperatures, which once again proves that Zn and Mg are difficult to separate, and other impurity metal gas content is far from the liquid, and we compared with the gas-liquid phase content, it was observed that Al, Ca, Cu, Ni, and Pb were numerous existent of in the liquid phase. Therefore, they are not volatile and remain in the liquid phase. For Fe, Mn, and other impurities, the gas-liquid equilibrium diagram cannot be calculated due to the lack of parameters. However, it can be seen from the phase diagram that the binary system Mg-Mn and Mg-Fe form an impossible alloy phase in the temperature range of 873–1073 K; they also have low solubility in magnesium and separate easily. Synthesizing the above theoretical analysis, the vacuum method can effectively recover magnesium and separate impurity metals.

Table 1. The separation coefficients of impurities at different temperatures [26].

T/K	873	923	973	1023	1073
β_{Al}	1.750×10^{-10}	6.383×10^{-10}	2.245×10^{-9}	6.757×10^{-9}	1.145×10^{-8}
β_{Zn}	0.894	0.851	0.9031	0.91	0.908
β_{Ca}	7.836×10^{-7}	1.599×10^{-6}	3.314×10^{-6}	6.223×10^{-6}	9.455×10^{-6}
β_{Cu}	9.783×10^{-13}	5.891×10^{-12}	3.248×10^{-11}	1.465×10^{-10}	1.848×10^{-9}
β_{Ni}	3.207×10^{-18}	3.564×10^{-17}	3.417×10^{-16}	2.535×10^{-15}	2.235×10^{-15}
β_{Pb}	3.503×10^{-7}	6.544×10^{-7}	9.735×10^{-7}	2.198×10^{-6}	3.378×10^{-6}

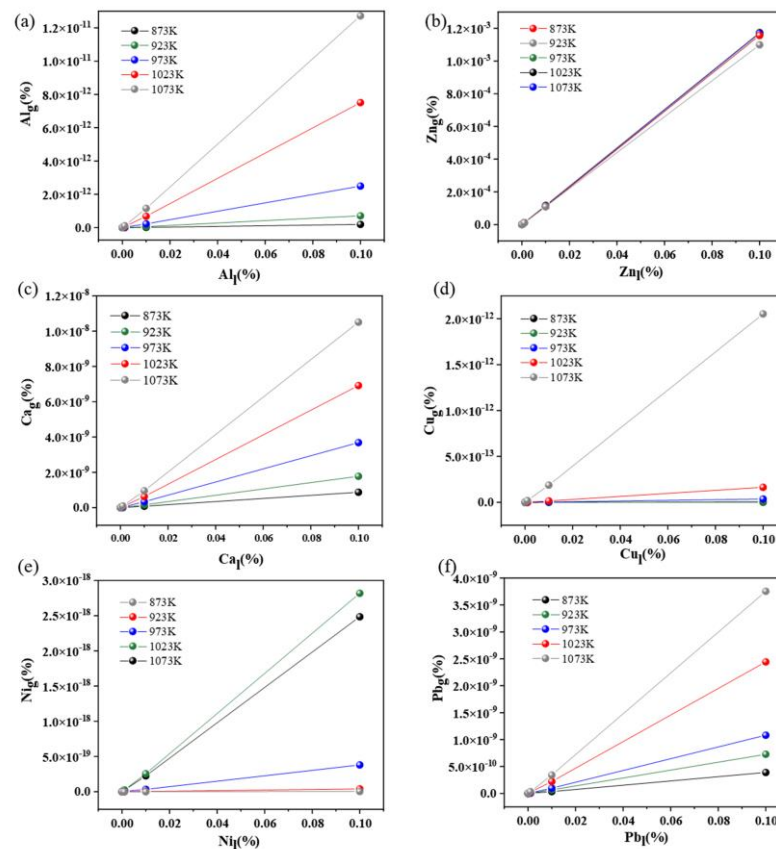


Figure 2. The gas-liquid equilibrium diagrams of impurities ((a) Al, (b) Zn, (c) Ca, (d) Cu, (e) Ni, (f) Pb).

3. Materials and Methods

3.1. Materials

The experimental raw material is Shanxi magnesium alloy scrap; the content of large impurity metals are mainly Al, Zn, and Mn, which are 6.14%, 0.24%, and 0.17%, respectively. The type and content of impurities in magnesium ingots as shown in Table 2.

Table 2. Type and content of impurities in magnesium ingots (wt.%).

Elements	Al	Zn	Mn	Si	Cu	Fe	Ni	Others
Raw Material	6.140	0.240	0.170	0.080	0.008	0.004	0.001	0.010

3.2. Method

We weighed 10 g of magnesium alloy and wiped the surface of the sample with sandpaper and alcohol, which can remove the surface oxidation layer and oil stains. Subsequently, the pretreated sample was placed in a graphite crucible, and the crucible was placed in the mouth of a quartz tube with a length, outer diameter, and thickness of 1200 mm, 50 mm, and 3 mm, respectively. Then the crucible was pushed into the heating zone with a pusher, and the mouth of the tube was sealed. The furnace pressure was pumped to a vacuum below 5 Pa, filled with argon gas, and the pressure was raised to 100 Pa. At the end of the experiment and after the furnace temperature had reached room temperature, the flange was opened, and the volatiles on the graphite paper and the residues in the crucible were collected, weighed, and sampled. Finally, the morphology of the magnesium condensation products was observed by scanning electron microscopy (SEM, Tescan Mira, Tescan, Brno, Czech Republic), and the purity of the condensates were characterized by inductively coupled mass spectrometry (ICP-MS, 7800(MS), Agilent, Santa Clara, CA, USA).

4. Results and Discussion

4.1. Effect of Distillation Temperature on the Purity of Magnesium

A total of 10 g of magnesium alloy was carried out on the vacuum method. The distillation temperature was 873–1073 K, system pressure was maintained at 100 Pa, and distillation time was 30 min. The influence of the distillation temperature was studied on magnesium volatilization, and magnesium alloy could be purified as much as possible. The index of the post-experiment evaluation was expressed by volatilization yield and direct yield.

$$\text{Volatilization yield(\%)} = \frac{m_{\text{raw material}} \times w_{\text{Mg,raw material}} - m_{\text{residual}} \times w_{\text{Mg,residual}}}{m_{\text{raw material}} \times w_{\text{Mg,raw material}}} \quad (5)$$

$$\text{Direct yield(\%)} = \frac{m_{\text{condensate}} \times w_{\text{Mg,condensate}}}{m_{\text{raw material}} \times w_{\text{Mg,raw material}}} \quad (6)$$

where $w_{\text{Mg,raw material}}$ is the content of magnesium in the raw material, %; $w_{\text{Mg,condensate}}$ is the content of magnesium in the condensation product on graphite paper, %.

Figure 3 shows the relationship between magnesium purity, direct yield, volatilization yield, and distillation temperature. As can be seen, the volatilization yield, direct yield, and purity of magnesium increase with the increase in temperature, which indicates that the increased temperature is beneficial to the purified magnesium alloys. Under certain pressure, a change in temperature affects the saturated vapor pressure and volatilization yield of magnesium. The higher the temperature, the greater the saturated vapor pressure of magnesium and the higher the volatilization yield. When the distillation temperature rises from 873 to 1023 K, the volatilization yield of magnesium increases significantly, from 2.93% to 96.32%, and the rising speed is fast. This is because, with the increase in temperature, the molecular diffusion speed is accelerated, the thermal motion is intensified, and the number of molecules that volatilize into the gas phase increases. The temperature continued to

increase. However, the rise gradually slowed down. This phenomenon occurs because with the increase in temperature, the volatile gas molecules volatilize completely. At this time, the non-volatile impurities gradually occupy the evaporation surface, thus reducing the number of molecules that evaporate on the surface, resulting in a lower volatilization rate. The direct yield of magnesium also increases with the increase in temperature. When the temperature exceeds 1023 K, the direct rate of magnesium gradually slows down. At 1073 K, it reaches a maximum of 98.62%, and the purity of magnesium alloys has a linear relationship with temperature. When the distillation temperature rises from 873 K to 1073 K, the purity of magnesium increases from 99.2% to 99.87%. As the temperature continues to rise, the purity remains unchanged.

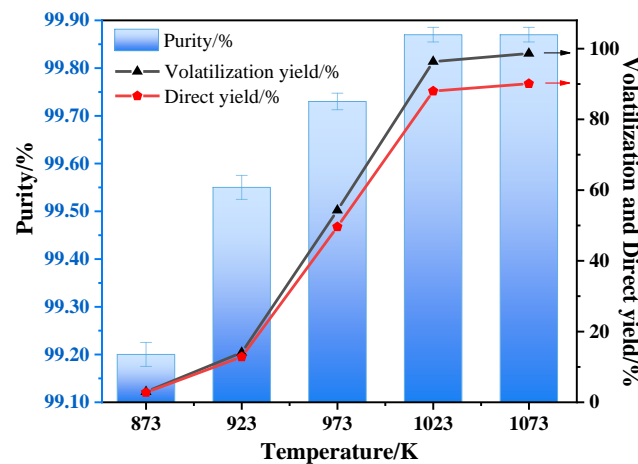


Figure 3. Magnesium purity, direct yield, and volatilization in relation to distillation temperature.

Meanwhile, the content of impurities such as Al, Zn, Mn, Cu, Fe, Ni, and Si in the residue of magnesium alloy in Figure 4, it can be seen that the contents of other impurities (except for Zn) increase with the increase in the distillation temperature. The results show that with the increase in temperature, impurities tend to gather in the residue, residue enrichment rate is the highest at 1073 K. At this time, the impurity content reaches 97.048% in the residue, the same as theoretical. All impurities (except Zn) were aggregated in the liquid. On the contrary, the content of Zn impurity decreases with the increase in the distillation temperature. This behavior is dominant when the temperature exceeds the melting point of Zn, which is 693 K, Zn will volatilize in gaseous form without enrichment in residues, and this process will be combined with Mg. Therefore, when the temperature is increased to 1073 K, the impurity contents are most enriched in the residue.

Figure 5 shows the effect of distillation temperature on the crystallization products by comparing the morphology of the crystallization products, when the temperature was constant, the size and morphology of the crystallization products varied, and the morphology of the particles changed from large hexagonal particles to powder, which indicates that the temperature affected the morphology of the crystallization products. It can also be seen that the temperature is 1073 K, the particles of crystallization products are fuller, with a particle size of 1447.4 μm , and the arrangement between the particles is more compact with non-existent gaps. On the contrary, at 873 K, the particle size of the crystallization product is relatively small, the size is 890.6 μm , and the arrangement is sparse with multiple gaps. Interestingly, when the temperature is 1073 K, the condensed magnesium obtained has the best purity and larger particle size. This is consistent with Xiong's statement that the condensate with high purity has a large particle shape [27]. Therefore, we believe that products with better crystalline morphology and larger particle size exist at higher temperatures. In summary, obtaining high-purity magnesium alloys is more favorable when the distillation temperature is 1073 K.

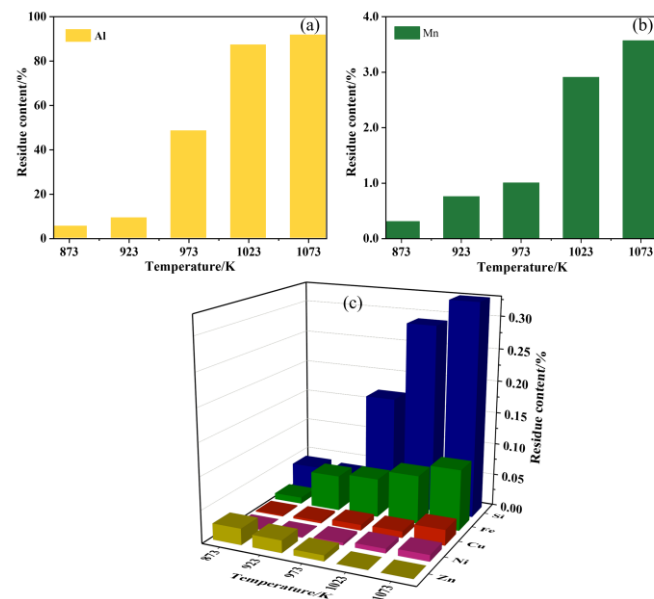


Figure 4. Main impurity contents in Mg residues at different temperatures ((a) Al impurity content; (b) Mn impurity content; (c) Other impurity contents).

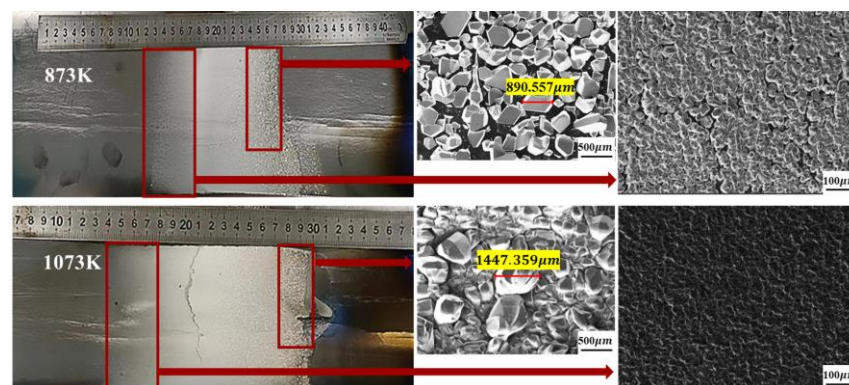


Figure 5. SEM images of the products in higher and lower distillation temperatures (873, 1073 K).

4.2. Effect of Condensation Temperature on the Purity of Magnesium

From the previous experiment, it can be seen that the distillation temperature was 1073 K. Although the purity of magnesium was improved, the effect was not significant. It is obvious that the purity of Mg cannot be improved effectively because Zn impurities cannot be separated effectively from Mg. According to the theoretical analysis, the melting point and saturated vapor pressure of Mg and Zn are very close, and the separation coefficient is close to 1. It is difficult to separate. Interestingly, the study found that Zn tends to concentrate at the cold end, which can be explained by thermodynamic theory analysis. Therefore, we use this characteristic to drive Zn to a lower temperature by using the directional condensation method, while Mg will concentrate a large amount at a higher condensation temperature so as to ensure the effective separation of Mg and Zn. According to the simulation of the obtained magnesium condensation zone temperature, when the condensation temperature was set to 723 K, 773 K, 823 K, and 873 K, the pressure was 100 Pa, the distillation temperature was 1073 K, and the holding time was 30 min. The experimental results are shown in Figure 6. With the increase in condensation temperature, the volatilization yield increases, but the trend is gradually slow. At the same time, the purity of the magnesium condensation product also increases continuously. When the condensation temperature rises from 723 K to 873 K, the purity of magnesium increases from 99.84% to 99.98%. The purity of the condensate product is the best when the condensation

temperature is 873 K. This phenomenon shows that the condensation temperature is one of the important factors that affect the purity of magnesium. In addition, condensation temperature has an important impact on the distribution and morphology of condensation products. We found that condensation products with different particle sizes are formed at different condensation temperatures, and the condensed crystallization quality is different.

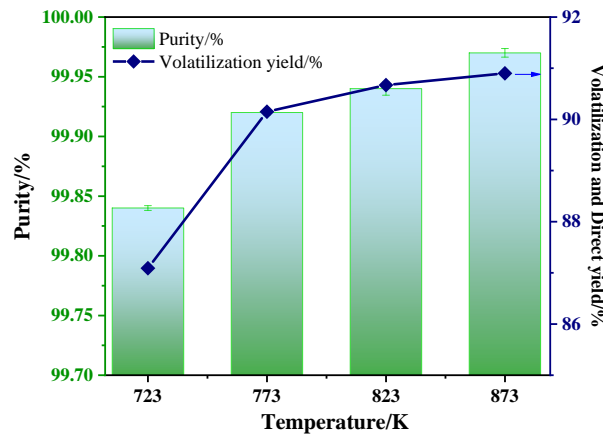


Figure 6. The purity and volatility of magnesium in relation to the condensing temperature.

Based on the optimal selection of the above experimental conditions, 10 g of magnesium alloy was used as the raw material, the system pressure was 100 Pa, the distillation temperature was 1073 K, the condensation temperature was 873 K, and the experiment was carried out for 30 min. The experimental results are shown in Figures 7–9 and Table 3.

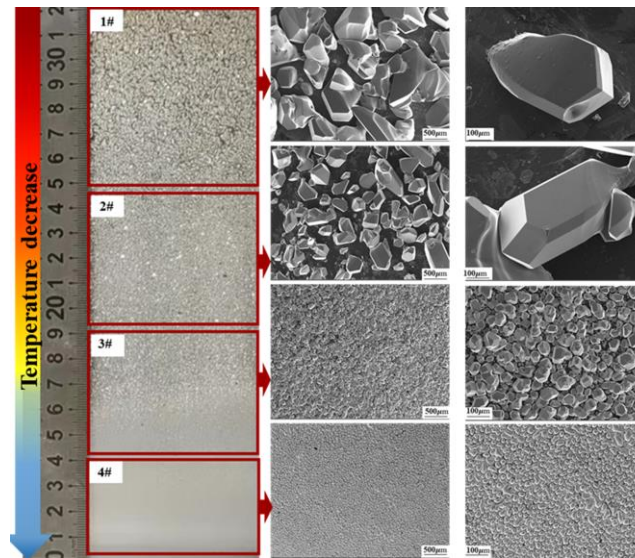


Figure 7. Graphite paper condensation product maps and SEM images of different condensation regions.

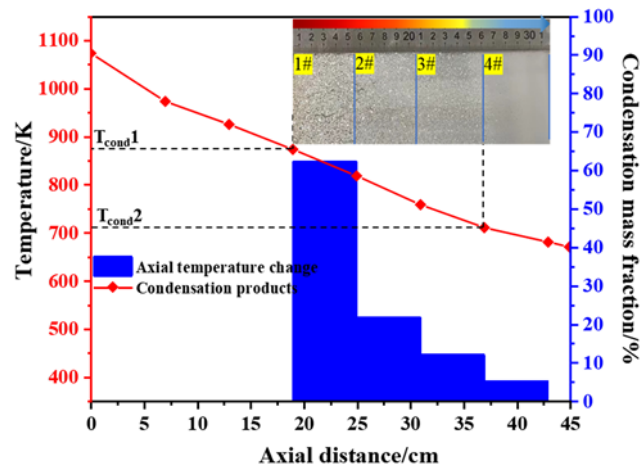


Figure 8. Axial temperature and condensation mass fraction as a function of axial distance (P = 100 Pa; T0 = 1073 K; T1 = 873 K; t = 30 min).

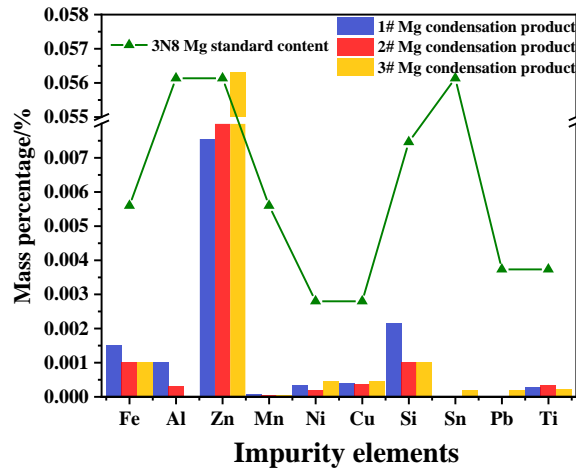


Figure 9. Contrast chart of the standard with the impurity compositions obtained after 30 min distillation at 1073 K and condensation at 873 K under vacuum (100 Pa).

Table 3. Comparison of 3N8 national standard and graphite paper condensate purity (wt.%).

Element	Content	1#	2#	3#	3N8 Standard Content
Fe		1.51×10^{-3}	1.00×10^{-3}	1.00×10^{-3}	2.00×10^{-3}
Al		1.01×10^{-3}	3.08×10^{-4}	1.82×10^{-3}	4.00×10^{-3}
Zn		7.55×10^{-3}	1.48×10^{-2}	5.63×10^{-2}	4.00×10^{-3}
Mn		7.50×10^{-5}	5.00×10^{-5}	5.00×10^{-5}	2.00×10^{-3}
Ni		3.39×10^{-4}	1.98×10^{-4}	4.52×10^{-4}	5.00×10^{-4}
Cu		4.00×10^{-4}	3.80×10^{-4}	4.50×10^{-4}	5.00×10^{-4}
Si		2.15×10^{-3}	1.00×10^{-3}	1.00×10^{-3}	3.00×10^{-3}
Sn		2.00×10^{-5}	2.19×10^{-5}	1.92×10^{-4}	4.00×10^{-3}
Pb		2.00×10^{-5}	2.19×10^{-5}	1.92×10^{-4}	1.00×10^{-3}
Ti		2.90×10^{-4}	3.44×10^{-4}	2.28×10^{-4}	1.00×10^{-3}
Mg		99.9881	99.9828	99.9393	99.9800

Figure 7 shows the magnesium condensation products on graphite paper and the scanning electron microscope on graphite paper. Condensate products of 1#, 2#, 3# and 4# are attached to graphite paper. The condensate product area is divided from the low-temperature zone to the high-temperature zone. In the figure, the magnesium condensation

products are silvery-white and form different morphology and crystal structure under temperature variation. The area where the highest temperature occurs is called 1#, and the shape is hexagonal large-sized particles with shimmering metallic luster. With the decrease in temperature, the graphite paper 2#, 3#, 4# condensation products shape gradually become smaller, and from small size hexagonal particles to oval particles, the surface gloss becomes darker. This is due to the lowering of the temperature to generate small dense particles of condensate, resulting in increased specific surface area, and oxidation tends to be severe. Therefore, increasing the condensation temperature can effectively increase the purity of magnesium and reduce the degree of oxidation

Figure 8 shows axial temperature and condensation mass fraction as a function of axial distance. It was divided into areas of 5.5 cm. As can be seen from the figure, the purity of the three condensation areas is above 99.9%, with a condensation distance range from 19.5 cm to 36 cm and a temperature range is 873–710 K at a system pressure of 100 Pa. Meanwhile, the axial distance of the condensation region is uniformly distributed, and with the decrease in temperature, the axial mass distribution on graphite paper is also from high to low, which are 61.98%, 21.42%, 11.78%, and 4.82%, respectively, and it depends on the decline of the saturation vapor pressure of magnesium within this region that is influenced by the temperature decrease within it. As the vapor pressure increases approximately with temperature and the temperature decrease is approximately linear within the four regions, the mass of condensate declines from region 1 with the highest temperature to region 4 with the lowest.

Table 3 and Figure 9 shows the comparison between the impurity contents of the national standard sample and with the vacuum of 100 Pa, distillation time of 30 min, distillation temperature of 1073 K, and condensation temperature of 873 K. As shown in Figure 9, the inductively coupled plasma mass spectrometer (ICP-MS) detected that the purity of the magnesium condensation products in the condensation zone of 1#, 2#, and 3# all reached 99.9%, where the position of 1# had the highest purity of magnesium, and combined with the SEM images in Figure 7, the region with the high temperature can obtain a higher purity of the condensation products [28–30]. The main reason for this phenomenon is that condensation temperature affects the crystallization nucleation process of magnesium condensation products. As the condensation temperature decreases, the number of magnesium vapor molecules decreases in the furnace, leading to a decrease in the number of atoms needed for nucleation, and eventually, the magnesium condensation products which are far from the heat source are powdery, while the condensation products closest to the heat source obtain the best crystallization and the highest purity. As can be seen from Table 3, the international standard of 99.98% was achieved for all impurity elements (except for zinc), but the content of zinc also decreased significantly, its content dropped from 0.450% to 0.056%. This shows that the vacuum method can effectively reduce the difficulty of removing zinc impurities. For the magnesium alloy with high zinc content, the zinc content can be reduced by multiple distillations to reach the standard of high-purity magnesium.

5. Conclusions

In summary, this paper studies the thermodynamic theoretical basis of magnesium and impurity metals, the factors which affect the vacuum gasification recovery experiment of waste magnesium alloy were discussed, and the specific conclusions are as follows:

- (1) Based on the saturated vapor pressure and the corresponding separation coefficients, it was determined whether the impurity elements in the magnesium alloy scrap were removed by the vacuum—gasification method. It was found that Mg and Zn were difficult to be separated. However, in this experiment, directional condensation is used to control the Zn crystallization region, which was reduced significantly from 0.45% to 0.056%.
- (2) Distillation temperature and condensation temperature have a significant impact on the purification of magnesium alloys and the morphology of condensation products.

- When the temperature gradient is different, the condensation purity of magnesium is different, and the morphology and crystal structure of magnesium condensate is different as well. The higher the temperature was, the better the crystallization of the condensate and the fuller the particles were. This is also true for purity. At a condensation temperature of 873 K, the condensation product reached 99.98% purity.
- (3) Magnesium alloys were purified by vacuum gasification—directional condensation method. Under the conditions of a distillation temperature of 1073 K, a condensation temperature of 873 K, a system pressure of 100 Pa, and a duration of 30 min, 3N8 high-purity magnesium was obtained at one time. Except for zinc content, other impurity elements all meet the 3N8 international standard.

Author Contributions: Investigation, R.L. and L.W.; Simulation, R.L.; Data curation, R.L.; writing-original draft preparation, R.L. and L.W.; methodology, Y.T. and B.Y.; supervision, B.X. and D.L.; writing-review and editing, Y.T. and F.W. All authors have read and agreed to the published version of the manuscript.

Funding: This research received no external funding.

Data Availability Statement: Not applicable.

Acknowledgments: The author gratefully Yang Tian for supporting the experimental study, Lipeng Wang and Dong Liang for the discussion of the theoretical analysis of thermodynamics, and Bin Yang, Baoqiang Xu, and Fei Wang for the guidance of the experimental results analysis.

Conflicts of Interest: The authors declare no conflict of interest.

References

- Liu, X.Y.; Mao, P.L.; Zhou, L.; Wang, X.T.; Wang, Z.; Wang, F.; Wei, Z.Q.; Liu, Z. Effect of Grain Size on Dynamic Compression Behavior and Deformation Mechanism of ZK60 Magnesium Alloy. *Metals* **2023**, *13*, 314. [\[CrossRef\]](#)
- Zhang, Z.Y.; Zhang, J.; Zhao, X.Y.; Cheng, X.Q.; Jiang, S.M.; Zhang, Q.F. Effects of Al-Mg on the Microstructure and Phase Distribution of Zn-Al-Mg Coatings. *Metals* **2023**, *13*, 46. [\[CrossRef\]](#)
- Wu, C.L.; Xie, W.J.; Man, H.C. Laser additive manufacturing of biodegradable Mg-based alloys for biomedical applications: A review. *J. Magnes. Alloy* **2022**, *10*, 915–937. [\[CrossRef\]](#)
- Shahin, M.; Wen, C.; Munir, K.; Li, Y.C. Mechanical and corrosion properties of graphene nanoplatelet-reinforced Mg–Zr and Mg–Zr–Zn matrix nanocomposites for biomedical applications. *J. Magnes. Alloy* **2022**, *10*, 458–477. [\[CrossRef\]](#)
- Jiang, J.H.; Xue, G.; Zhang, X.B. Mechanical and Corrosion Properties of Mg–Gd–Cu–Zr Alloy for Degradable Fracturing Ball Applications. *Metals* **2023**, *13*, 446. [\[CrossRef\]](#)
- Hussein, M.A.; Azeem, M.A.; Kumar, A.M.; Emara, N.M. Processing and in vitro corrosion analysis of sustainable and economical eggshell reinforced Mg and Mg-Zr matrix composite for biomedical applications. *Mater. Today Commun.* **2022**, *32*, 103944. [\[CrossRef\]](#)
- Zhou, H.; Liang, B.; Jiang, H.T.; Deng, Z.L.; Yu, K.X. Magnesium-based biomaterials as emerging agents for bone repair and regeneration: From mechanism to application. *J. Magnes. Alloy* **2022**, *9*, 779–804. [\[CrossRef\]](#)
- Lee, S.I.; Lee, J.H.; Park, S.H. Static strength test with as-forged control-arm in automobile with Mg-Al-Sn-Zn alloy. *J. Mech. Sci. Technol.* **2016**, *30*, 3793–3798. [\[CrossRef\]](#)
- Tong, F.L.; Chen, X.Z.; Wei, S.H.; Malmström, J.; Vella, J.; Gao, W. Microstructure and battery performance of Mg-Zn-Sn alloys as anodes for magnesium-air battery. *J. Magnes. Alloy* **2021**, *9*, 1967–1976. [\[CrossRef\]](#)
- Zhang, K.; He, Y.Z.; Dong, Z.R. Pulsed Eddy Current Nondestructive Testing for Defect Evaluation and Imaging of Automotive Lightweight Alloy Materials. *J. Sens.* **2018**, *2018*, 1639387. [\[CrossRef\]](#)
- Lee, S.E.; Kim, M.S.; Chae, Y.W. Effect of intermediate heat treatment during hot rolling on the texture and formability of annealed AZ31 Mg alloy sheets. *J. Alloys Compd.* **2022**, *897*, 163238. [\[CrossRef\]](#)
- Lisabeth-Riopelle, B.S. The recycling of magnesium makes cents. *JOM* **1996**, *48*, 44–46. [\[CrossRef\]](#)
- Cao, H.X.; Huang, M.T.; Wang, C.C.; Long, S.Y.; Zha, J.L.; You, G.Q. Research status and prospects of melt refining and purification technology of magnesium alloys. *J. Magnes. Alloy* **2019**, *7*, 11. [\[CrossRef\]](#)
- Hu, M.L.; Ji, Z.S.; Chen, X.Y. Effect of extrusion ratio on microstructure and mechanical properties of AZ91D magnesium alloy recycled from scraps by hot extrusion. *T Nonferr. Metal. Soc.* **2010**, *20*, 987–991. [\[CrossRef\]](#)
- Inoue, M.; Doi, T.; Aida, T.; Matsuki, K.; Kamado, S.; Kojima, Y. Vacuum Distillation Refining and Extrusion Process of Magnesium. *Mater. Sci. Forum* **2005**, *475–479*, 513–516. [\[CrossRef\]](#)
- Lucci, R.; Padilla, L.R.; Cantero, S.; Bariles, R.; Oldani, C. Refining of AZ91 Magnesium Alloy Obtained in Machining Chips Recycling. *Procedia Mater. Sci.* **2015**, *8*, 886–893. [\[CrossRef\]](#)

17. Le, Q.C.; Zhang, Z.Q.; Cui, J.Z.; Chang, S.W. Study on the Filtering Purification of AZ91 Magnesium Alloy. *Trans Tech Publ.* **2009**, *610–613*, 754–757. [[CrossRef](#)]
18. Rambabu, U.; Munirathnam, N.R.; Prakash, T.L. Purification of gallium from Indian raw material sources from 4N/5N to 6N5 purity. *Mater. Chem. Phys* **2008**, *112*, 485–489. [[CrossRef](#)]
19. Zhang, X.W.; Wang, Z.Q.; Chen, D.H.; Li, Z.G.; Miao, R.Y.; Yan, S.H. Preparation of High Purity Rare Earth Metals of Samarium, Ytterbium and Thulium. *Rare Met. Mater. Eng.* **2016**, *45*, 2793–2797.
20. Zhang, Y.K.; Lei, Y.; Ma, W.H.; Wang, H.; Hu, Y.Q.; Wei, K.X.; Li, S.Y. Preparation of high-purity Ti–Si alloys by vacuum directional solidification. *J. Alloys Compd.* **2020**, *832*, 153989. [[CrossRef](#)]
21. Liang, D.; Tian, Y.; Yang, B.; Xiong, N.; Wang, F.; Xu, B.Q. One-step preparation of high purity magnesium by vacuum distillation technology. *Vacuum* **2021**, *192*, 110464. [[CrossRef](#)]
22. Ali, S.T.; Munirathnam, N.R.; Sudheer, C.; Reddy, R.C. Prakash, Purification of cadmium by vacuum distillation and its analysis. *Mater. Lett.* **2004**, *58*, 1638–1641. [[CrossRef](#)]
23. Tian, Y.; Zhang, X.P.; Qu, T. Technical research on vacuum distillation to purify magnesium to 99.99% purity. *Mater. Res. Express* **2021**, *8*, 056506. [[CrossRef](#)]
24. Li, Q.; Hu, Z.F.Z.; Li, Q. High purity magnesium was prepared by vacuum distillation. *Nonfer. Metals* **2014**, *6*, 21–23.
25. Dai, Y.N.; Yang, B. *Non-Ferrous Metal Vacuum Metallurgy*; Beijing Metallurgical Industry Press: Beijing, China, 2009; pp. 34–46.
26. Wang, Y.C. *Study on Preparation of High Purity Magnesium by Vacuum Distillation*; Kunming University of Technology: Kunming, China, 2014; Volume 4.
27. Xiong, N.; Tian, Y.; Yang, B.; Xu, B.Q.; Liu, D.C.; Dai, Y.N. Volatilization and condensation behaviours of Mg under vacuum. *Vacuum* **2018**, *156*, 463–468. [[CrossRef](#)]
28. Han, J.B.; Zhang, T.A.; Fu, D.X.; Guo, J.H.; Zhou, H.J.; Dou, Z.H. Condensation Behavior of Magnesium Metal in Argon Gas. *Metal. Mater. Trans. B* **2020**, *51*, 3098–3107. [[CrossRef](#)]
29. Han, J.B.; Fu, D.X.; Guo, J.H.; Zhou, H.J.; Zhang, T. Volatilization and condensation behavior of magnesium vapor during magnesium production via a silicothermic process with magnesite. *Vacuum* **2021**, *189*, 110227. [[CrossRef](#)]
30. Han, J.B.; Fu, D.X.; Guo, J.H.; Zhou, H.J.; Dou, Z.H.; Zhang, T. Nucleation and Condensation of Magnesium Vapor in Argon Carrier. *Metals* **2020**, *10*, 1441. [[CrossRef](#)]

Disclaimer/Publisher’s Note: The statements, opinions and data contained in all publications are solely those of the individual author(s) and contributor(s) and not of MDPI and/or the editor(s). MDPI and/or the editor(s) disclaim responsibility for any injury to people or property resulting from any ideas, methods, instructions or products referred to in the content.